ELSEVIER

International Journal of Mass Spectrometry 212 (2001) 477–489

International Journal of Mass Spectrometry

www.elsevier.com/locate/ijms

Sputtering of condensed polyatomic gases by kilo-electron-volt-energy ions

Donald E. David[a], V. Balaji[a], Josef Michl[a,*], Herbert M. Urbassek[b]

[a]*Department of Chemistry and Biochemistry, University of Colorado, Boulder, CO 80309-0215, USA*
[b]*Physics Department, University, D-67663 Kaiserslautern, Germany*

Received 22 May 2001; accepted 20 August 2001

Abstract

We have measured the initial and fluence-dependent sputtering yields of condensed neat CO_2, NO_2, N_2O, CH_4, C_2H_4, and NH_3 for kilo-electron-volt-energy rare-gas ion bombardment. The results of the measurements are rationalized in terms of the gas-flow model of condensed-gas sputtering, modified by the chemical reactions expected to occur during and after gas flow. The three triatomic target molecules studied have similar physical properties. The different initial sputtering yields observed are rationalized in terms of chemical effects occurring during bombardment. Only moderate fluence dependencies are observed. Sputtering of CH_4 and C_2H_4 targets occurs with only moderate initial sputtering yields, compatible with no gas-flow participation in the sputtering mechanism. With increasing incident ion fluence, the sputtering yields rise due to the build up of highly volatile products. For higher bombardment fluences two different results are observed. In the case of lighter bombarding ions (He^+, Ne^+, and, for the C_2H_4 target, also Ar^+) the yields eventually decrease, probably due to polymerization reaction products coating the target. For heavier projectile ions the yields plateau at a high level. We attribute this latter behavior to a strong gas-flow contribution which entraps even the heavier carbonaceous products in the gas flow and prevents their accumulation on the surface. This behavior has not been observed before. The sputtering behavior of NH_3 follows closely that of CH_4, except that yield decreases due to polymerization are absent. (Int J Mass Spectrom 212 (2001) 477–489) © 2001 Elsevier Science B.V.

1. Introduction

The interaction of energetic ions with condensed gases is of interest for several disciplines, primarily for the planetary sciences [1] and ion beam inertial fusion [2]. It also attracts fundamental interest as a case study for chemical sputtering [3] and reactive ion etching [4] processes. Furthermore, the huge sputtering yields found for these materials establish them as prototypical examples of the effect of thermal (elastic collision) spikes on sputtering [5]. Because the cohesive energies of the condensed gases are so small, similar effects in other materials can be achieved only under quite special bombardment conditions, such as cluster impact [6].

Many previous studies of condensed-gas sputtering concentrated on high bombarding energies, in the upper kilo-electron-volt (keV) and mega-electron-volt (MeV) ranges, where the effects of electronic excitation are significant or even dominant and give rise to electronic sputtering [7]. Sputtering yield studies in the low-keV regime, such as those covered in the

* Corresponding author. E-mail: michl@eefus.colorado.edu

Dedicated to R. Graham Cooks on the occasion of his sixtieth birthday.

PII S1387-3806(01)00528-0

present article, have been performed on both condensed rare gas [8] and diatomic gas targets [9]. The overall picture that has emerged from these investigations is the following: the primary ion energy is quickly dissipated by a collision cascade among target atoms or molecules. The energy density created in the collision cascade volume may be relatively high, surpassing the intermolecular binding forces of the material. Consequently, some of the gasified collision cascade volume flows out into the vacuum, giving rise to a considerable ejection yield, one much too large to be explained by collision cascade sputtering alone. Three similar mechanisms have been suggested to account for this enhanced yield: the thermal spike [10], reduction in intermolecular bonding [11], and the gas-flow mechanism [12–15]. We employ the latter, since it appears plausible for condensed gases and accounts successfully for the results obtained on monoatomic [8] and diatomic [9] targets. The products which are formed by molecular dissociations in the collision-cascade stage may react rapidly with the surrounding target gas during gas flow. The exothermicity of these reactions adds an amount of energy to the gas flow that can be, in some cases, even larger than the amount initially used to dissociate molecules. This chemical energy correlates well with the observed increased sputtering yield for molecular targets relative to atomic ones. Further, it appears that molecular targets are chemically modified by the inclusion of some portion of the reaction products in the target after bombardment, giving rise to a fluence dependence of the sputtering yield.

We have chosen to study three triatomic gases (CO_2, NO_2, and N_2O) as sputtering targets. Since their physical characteristics are quite similar, their differing sputtering behavior can be interpreted in terms of the chemistry occurring during and after ion impact. We have also chosen to study three hydrogen-rich molecules (CH_4, C_2H_4, and NH_3). Their sputtering behavior is characterized by a considerable fluence dependence, which in the case of CH_4 and C_2H_4 is due to a competition between polymerization reactions suppressing sputtering and the gas-flow mechanism enhancing it.

2. Experiment

Sputtering yields were measured as a function of incident ion fluence on the same instrument previously used to study sputtering of several condensed diatomic gases [9]. The instrument consists of two heterodyned 6 MHz quartz crystal microbalances mounted at the end of a liquid helium cryostat such that the target gas is deposited on one microbalance while the other is protected and serves as a reference. The difference frequency is measured with a MetraByte timer-counter data acquisition card (Model CTM-05) mounted in a PC-type computer which records and manipulates the data. The ion source is a Leybold-Heraeus ion gun (Model IQE 12/63), and the incident ion current is measured with a Keithley electrometer (Model 617) connected to the computer by way of an IEEE-488 interface. This system is thought to have a mass (and sputtering yield) accuracy of better than 10% and is able to detect a mass change as small as 40 pg/s, equivalent to 0.3% of a monolayer/s for a CO_2 target.

Each plotted data point represents the average yield over a 20 s measurement period (effectively instantaneous) at current densities smaller than 25 nA/cm^2. About 2×10^{18} molecules/cm^2 of each target gas were deposited at the annealing temperature (CO_2, 98 K; NO_2, 140 K; N_2O, 92 K; NH_3, 120 K; CH_4, 44 K; and C_2H_4, 74 K) and then cooled to 5 K for measurement. These conditions resulted in reproducible yields, independent of film thickness and temperature. Tests were done to ensure the absence of fast neutrals in the incident beam, uniform ion fluence over the active area of the microbalance, and the absence of surface charging and ion induced increases in the target temperature.

3. Results

The instantaneous sputtering yields Y for CO_2, NO_2, N_2O, NH_3, CH_4, and C_2H_4 bombarded by 5 keV

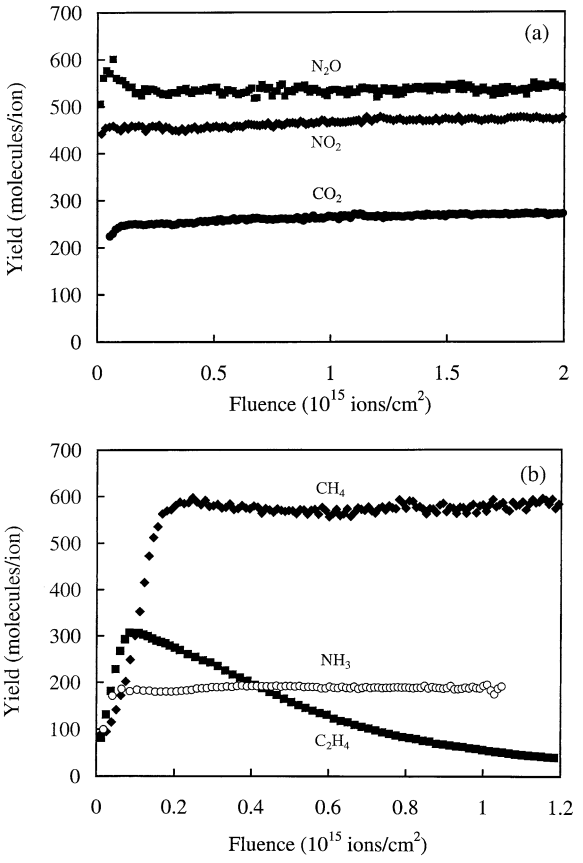

Fig. 1. Measured sputtering yield Y vs. fluence Φ_I for (a) solid CO_2, NO_2, N_2O, and (b) solid CH_4, C_2H_4, and NH_3 bombarded by 5 keV Ar^+ ions.

Ar^+ ions are plotted against incident ion fluence Φ_I in Fig. 1(a) and (b). It can be seen that in all cases Y depends on Φ_I. As observed previously for the diatomic targets O_2 and NO [9], the yields for CO_2, N_2O, NH_3, and CH_4 change rapidly for the first 2×10^{14} ions/cm^2 (approximately the fluence at which projectiles start hitting previously bombarded areas) and are then nearly constant. In contrast, the yield for NO_2 rises only very slowly, and for C_2H_4 it initially rises and then steadily decreases, reminiscent of the trend observed previously for CO [9] and even earlier for sputtering in the electronic-stopping regime [1,7].

For CO_2, NO_2, N_2O, and NH_3, (and also for all the diatomic targets measured previously [9]) the general shapes of the Y versus Φ_I curves were found to be

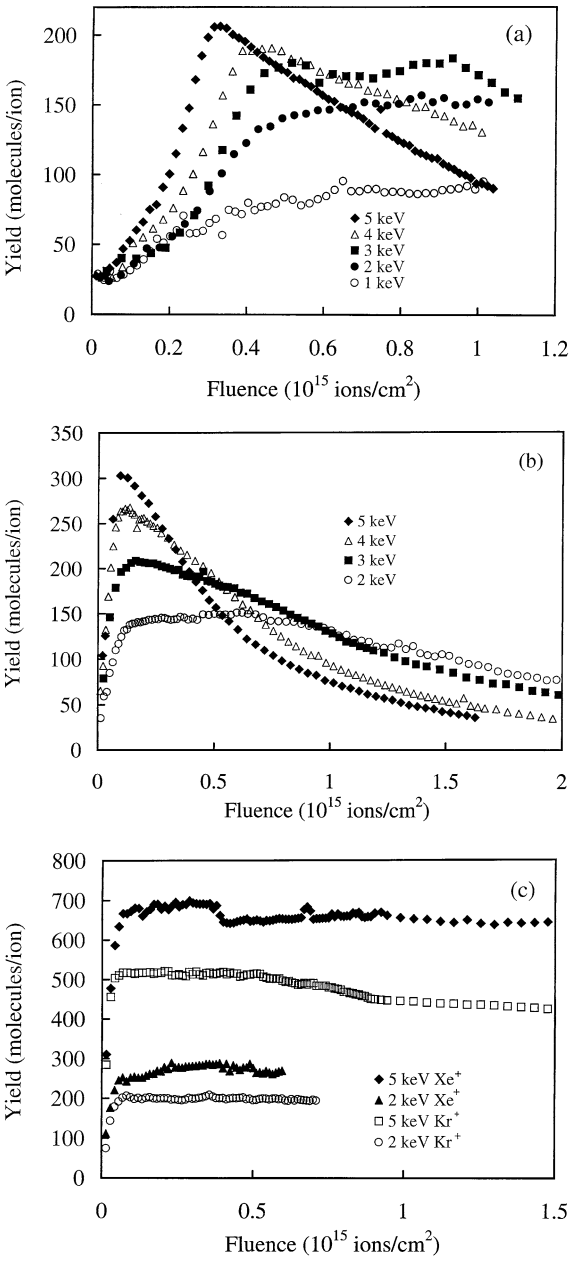

Fig. 2. Measured sputtering yield Y vs. fluence Φ_I for (a) solid CH_4 bombarded by 1–5 keV Ne^+ ions, (b) solid C_2H_4 bombarded by 1–5 keV Ar^+ ions, and (c) solid C_2H_4 bombarded by 2 and 5 keV Kr^+ and Xe^+ ions.

independent of the incident ion and energy. For the carbon rich targets CH_4 and C_2H_4, this is not the case. Fig. 2 is split into three plots of Y versus Φ_I for these

Table 1
Initial sputtering yields Y_0 for CO_2, N_2O, NO_2, CH_4, C_2H_4, and NH_3 bombarded by 1–5 keV rare-gas ions

E (keV)	He^+	Ne^+	Ar^+	Kr^+	Xe^+
CO_2					
1	15	38	64	80	104
2	17	64	130	146	148
3	19	84	176	197	231
4	20	106	210	261	304
5	22	127	233	325	381
N_2O					
1	30	79	95	101	108
2	39	146	219	215	264
3	47	209	306	308	408
4	55	268	394	414	538
5	60	310	516	522	672
NO_2					
1	27	76	103	117	118
2	30	153	224	262	298
3	35	196	302	418	410
4	39	239	374	531	545
5	45	264	442	683	691
CH_4					
1	...	27	57	62	80
2	6	26	87	126	147
3	7	33	92	145	202
4	5	25	93	168	239
5	28	30	94	175	274
C_2H_4					
1	...	...	...	20	32
2	...	...	35	75	111
3	...	...	79	186	222
4	...	...	65	193	283
5	...	...	104	284	310
NH_3					
1	4	33	36	43	41
2	6	36	54	58	109
3	6	40	59	143	172
4	8	...	82	166	182
5	18	45	100	176	203

targets for incident ions and energies that are selected to illustrate the different trends. Fig. 2(a) is for CH_4 bombarded by 1–5 keV Ne^+ ions, Fig. 2(b) is for C_2H_4 bombarded by 1–5 keV Ar^+ ions, and Fig. 2(c) is for C_2H_4 bombarded by 2 and 5 keV Kr^+ and Xe^+ ions. In general, it was found that Y always increases initially, but a subsequent decrease occurs only when the incident energy is high or the incident ion mass is large, i.e. when the yield is large. Measured initial sputtering yields Y_0 (effectively, $\Phi_I = 0$) are listed in Table 1.

4. Discussion

In the following, we provide a semiquantitative account of the observed initial sputtering yields Y_0 based on the gas-flow model [15] that explained successfully the sputtering of solid rare gases [8] and diatomic molecules [9], and a qualitative account of the changes in the sputtering yield Y as a function of fluence.

4.1. Collision cascade stage

The primary ion is slowed down in the target material by energetic collisions with the target mole-

Table 2
Quantities relevant to the sputtering of condensed gas targets by 5 keV Ar^+ ions (data taken from [29–32])

	M[a](u)	n[b](10^{-3} Å^{-3})	T_c[c](K)	U[d](meV)	S[e](eV Å^{-2})	Y_{casc}[f]	Y_0[g]	E_{chem}[h](eV)
CO_2	44	16.1	304	158	3.34	180	233	577
N_2O	44	16.8	310	171	3.28	163	516	1795
NO_2	46	19.0	430	395	3.38	70	442	1311
CH_4	16	16.0	191	85	1.02	96	94	79
C_2H_4	28	12.3	283	140	2.04	116	104	938
NH_3	17	24.1	406	242	1.06	38	100	−62

[a] M molecular mass.
[b] n molecule number density at boiling temperature T_b (with the exception of CO_2 where the triple point temperature is taken).
[c] T_c critical temperature.
[d] U surface binding energy (calculated from the heat of vaporization at T_b).
[e] S nuclear stopping power of entire molecule (cf. [9]).
[f] Y_{casc} collision-cascade contribution to sputtering (calculated).
[g] Y_0 initial sputtering yield (measured).
[h] E_{chem} ion-induced chemical energy release.

cules. These or their dissociation fragments recoil from the collision and start sharing their energy in further collisions. In this collision cascade, the primary ion energy E is spread out over the cascade volume $V \propto r^3$. A typical linear dimension (width or depth) of the volume scales as [9,16]

$$r \propto \frac{E}{nS} \tag{1}$$

where the proportionality constant depends slightly on the interaction potential and on the projectile/target mass ratio, n is the target molecule density, and S is the ion stopping cross section, which depends on ion energy as well as on the ion and target molecular species. Data for n and S are given in Table 2. Here we assume that the projectile/molecule collision can be considered as a spectator collision with one atom of the molecule, such that S can be calculated as the sum of individual atom–atom stopping cross sections. We note that part of the projectile energy will be lost in electronic excitations and ionization; this contribution is of minor influence except for He^+ ion bombardment and possibly for hydrogen-rich targets.

Sputtering is expected to occur during this energetic collision cascade phase with a yield of [16,17]

$$Y_{casc} = 0.076 \frac{\beta S}{C_0 U} \tag{2}$$

where U is the target sublimation energy, $C_0 = 1.8$ Å^2 is a constant, and β is a function of the projectile/target mass ratio, which assumes values around 0.25 in the cases of interest in this article. Table 2 shows the calculated values of Y_{casc}, which range up to 180, due to the low values of U.

4.2. Dissociation

As a result of energetic ion–molecule and recoil atom–molecule collisions occurring in the cascade volume, molecules may dissociate. Generalizing the ideas that we put forward earlier [9], let us consider a molecule of mass M, one of whose atoms (mass m) receives an energy E_{coll} in the course of the cascade. In a simple "spectator" collision model, valid for collision energies that are not too small, this means that the molecule receives an internal energy of $E_{int} = (M - m)/M \times E_{coll}$. The molecule can only break a bond of dissociation energy D if $E_{int} > D$, and it will be assumed that the break up is fast on our time scale. The number of dissociations induced by a primary ion of energy E can be estimated from collision cascade theory [16] to be

$$N_{diss} = \frac{M - m}{M} \Gamma_m \frac{E}{D} \tag{3}$$

Table 3
Number v_i of products i formed by bombarding a condensed-gas target by a 5 keV Ar^+ ion. Here X denotes a C or N atom and Y denotes an O or H atom, as appropriate; the dissociation energies D_{AB} for breaking bond A–B, and D_{tot} denoting the total atomization energy, were calculated from the pertinent reaction enthalpies

	D_{XY}(eV)	D_{XX}(eV)	D_{tot}(eV)	v_Y	v_X	v_{XY}	v_{XX}
CO_2	7.48	...	20.60	207	32	143	...
NO_2	5.14	...	13.64	271	38	194	...
N_2O	3.70	5.00	13.50	191	197	113	149
NH_3	4.71	...	7.63	375	14	...	...
CH_4	4.55	...	8.20	412	15	...	...
C_2H_4	4.81	10.89	...	333	44	44	...

where Γ_m is a cross-section parameter with value $\Gamma_m \simeq 0.5$, consuming a total energy of

$$E_{diss} = N_{diss}D \cong \frac{M-m}{2M}E \tag{4}$$

These ideas may be applied to triatomic molecules ABC (with end atoms A and C) as follows. The collision energy E_{coll} is given with probability 1/3 to atoms A. The number of dissociations of A–B bonds (with bond energy D_{AB}) to form atoms A and molecules BC is, in analogy to Eq. (3),

$$N_{AB} = \frac{1}{3}\frac{m_B + m_C}{M}\Gamma_m \frac{E}{D_{AB}} \tag{5}$$

The cases where atoms B or C receive the collision energy are handled analogously, with the assumption that for atoms B, both the A–B and the B–C bonds are broken. The same method can be extended to larger molecules by adjusting for the relative probabilities for each atom being struck and then summing the dissociation energy for each broken bond, again assuming that all bonds connected to the struck atom are broken.

From these expressions, the number v_i of products i formed in a cascade can be determined by summing up the respective numbers from the individual cases. The results for the six molecular targets studied here are listed in Table 3.

4.3. Gas flow

The collision cascade stage is over when the particle energy in the cascade volume has reached a quasiequilibrium. The temperature in the cascade volume can then be approximated by

$$T \propto \frac{E}{nr^3C} \propto \frac{S}{r^2C} \tag{6}$$

where C is the specific heat (at constant volume) of the target material. More precisely, we may write [9]

$$T = \frac{nS}{\pi C\rho^2} \tag{7}$$

Here, ρ is the lateral width of the cascade, which is given by stopping theory [15,16] as

$$\rho = 0.42\frac{E_0^{2m}}{nC_m} \tag{8}$$

and C_m denotes the so-called cross-section constant.

In most materials the temperature T will be far below the critical temperature T_c of the gas–liquid phase transition, such that after the collision cascade stage no further sputtering can occur. In condensed gases, however, T_c is low, and the condition $T > T_c$ is more easily reached. Then part of the energized cascade volume can flow out of the cascade volume before heat conduction to the surroundings causes the temperature to drop far enough to freeze the flow. For molecular solids, this typically occurs in a few hundred picoseconds. The corresponding contribution to sputtering has been termed [15] the gas-flow yield, Y_{gas}.

The gas-flow contribution to sputtering has been estimated [9] as

$$Y_{\text{gas}} = \frac{\sqrt{\pi}}{4}\,\xi^2 n\,\frac{r^4 T}{T_c} \tag{9}$$

where ξ is a fitting factor and denotes the fraction of the cascade surface area active in the gas flow. This formula is valid for $T \gg T_c$ and is the limiting case of a more general expression. Note that a dependence on T_c does not occur in other sputtering models. For the three triatomic gases considered, the physical properties collected in Table 2 are very similar. As a consequence T, and thus Y_{gas}, are expected to be very similar for these three targets, and from Eq. (9) we immediately obtain

$$\frac{Y_{\text{gas},X}}{Y_{\text{gas},\text{CO}_2}} = \frac{T_{c,\text{CO}_2}}{T_{c,X}} \tag{10}$$

This relation was observed in the case of those diatomic solids for which no net chemical transformations were expected [9] and can be expected to hold for the cases studied here in the absence of chemical reactions. In particular, the Y_0 values for CO_2 and N_2O should be identical, while that of NO_2 should be slightly smaller since T_c of the latter is somewhat larger. The experimental data reveal that this is not the case. We attribute this discrepancy to chemical effects occurring during the gas flow.

4.4. Effects of chemical reactions

In a manner similar to that discussed previously for diatomic targets [9], the atomic and molecular fragments formed during the collision cascade can either recombine or react with the surrounding molecules, altering the chemical composition of the bombarded material. The latter reactions are much more likely since only a few percent of the molecules in the collision cascade volume are dissociated and a fragment is more likely to encounter one of the surrounding molecules than another fragment during the few hundred picoseconds of gas flow. For instance, we neglect the effects of hydrogen atom recombination in the discussion of the sputtering of hydrocarbons and ammonia, even though it is known that most of them recombine ultimately (e.g. the energy release associated with hydrogen atom recombination causes an amorphous to crystalline transition in water ice [18]). We also dismiss reactions with significant activation energies as being too slow to affect the energy balance. For example, in the discussion of the sputtering of the three triatomic targets studied, we expect singlet (^1D) oxygen atoms to react with little or no activation energy while the corresponding reactions with ground state triplet (^3P) oxygen atoms proceed too slowly to be important (e.g. using O(^3P) atoms in reaction (21), where $A = 6.92 \times 10^{10}$ and $E_a = 28$ kcal/mol [19], should result in only about one reaction occurring per 5×10^4 incident 5 keV Ar^+ ions). In any case, the fragmentation reactions surely initially form O(^1D) atoms, the subsequent spin flip to give O(^3P) atoms must be slow on the time scale of gas flow, and thus O(^1D) atoms must predominate.

Consequently, we are primarily concerned with exothermic reactions that proceed with little or no activation barrier and occur between products of the collision cascade and the major surrounding material. These reactions add a maximum amount of chemical energy that can be estimated from

$$E_{\text{chem}} = -N_{\text{diss}}\Delta H_{\text{reac}} = -\frac{1}{4}\,\frac{\Delta H_{\text{reac}}}{D}\,E \tag{11}$$

where ΔH_{reac} is the net change in enthalpy for all reactions leading from the initially formed fragments to stable products on a time scale relevant to gas flow. This added energy counteracts heat losses and prevents early cooling and condensation of the gas, extending the duration of the sputtering process. For targets with similar physical properties one should expect that relative differences in yields would be related to E_{chem}. This idea is supported by Fig. 3, which plots Y_0 versus E_{chem} for the triatomic targets bombarded by 5 keV Ar^+ ions. Clearly, the yields do correlate with E_{chem}. The reactions used for computing E_{chem} are given below for each molecule and the results are presented in the following and in Table 2.

The fluence dependence of Y can be understood by examining the reaction products which are expected to build up in the target. When $\Phi_I > 0$, E_{chem} must be modified to include the additional reactions which

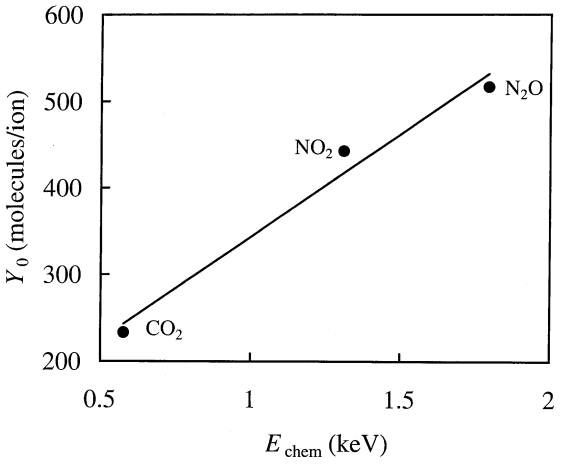

Fig. 3. Measured initial sputtering yield Y_0 vs. E_{chem} for solid CO_2, NO_2, and N_2O bombarded by 5 keV Ar^+ ions.

can occur between new products and the products formed by previous impacts and then frozen in the target. In addition, T_c for the reaction products that accumulate may be considerably different than T_c for the original target (e.g. T_c for NH_3 is 406 K but T_c for H_2, a major sputtering product, is 33 K). As a result, as Φ_I increases, we expect there to be a general tendency for Y to increase if products with low T_c accumulate in the target, but for Y to decrease if products with high T_c accumulate. In the following discussion, we refer specifically to results obtained for bombardment with 5 keV Ar^+ ions, but it is expected to apply generally. The specific reactions which contribute to E_{chem} and change the effective T_c of the target material are described in the following for each target (reaction heats are shown [20]):

4.4.1. CO_2

$$CO_2 \rightarrow CO + O(^1D) \qquad \Delta H = 7.48 \text{ eV} \qquad (12)$$

$$CO_2 \rightarrow C + 2O(^1D) \qquad \Delta H = 20.60 \text{ eV} \qquad (13)$$

$$O(^1D) + CO_2 \rightarrow O_2 + CO \qquad \Delta H = -1.62 \text{ eV} \qquad (14)$$

$$O(^1D) + CO_2 \rightarrow CO_3 \qquad \Delta H = -2.21 \text{ eV} \qquad (15)$$

$$C + CO_2 \rightarrow 2CO \qquad \Delta H = -5.64 \text{ eV} \qquad (16)$$

The neutral material sputtered from solid CO_2 by 6 keV Ar^+ ions has been reported [21,22] to be primarily CO and CO_2, whereas the negative ion products were dominated by CO_3^- anions [23]. These sputtered products are consistent with the reactions listed since CO_3 (electron affinity = 3.26 eV [20]) can be expected to scavenge much of the negative charge to form the observed anion. Assuming similar frequency factors for reactions (14) and (15), we calculate E_{chem} to be 577 eV [(207/2 O atoms × −1.62 eV) + (207/2 O atoms × −2.21 eV) + (32 C atoms × −5.64 eV)]. Experimentally, Y_0 is 233 molecules/ion, the smallest value of the three triatomic targets measured and is consistent with a relatively small E_{chem}. In fact, Y_0 is nearly the same as that predicted for Y_{casc}.

With increasing incident ion fluence, Y increases rapidly to 250 molecules/ion at $\Phi_I \simeq 2 \times 10^{14}$ ions/cm^2 and thereafter continues to rise only very slowly. We propose that the initial increase is due to reactions (12)–(16) and secondary reactions such as the combination of O atoms to form O_2, which enrich the surface in the more volatile products O_2 and CO. These molecules both have high sputtering yields (700 and 817 molecules/ion, respectively [9]). The slow rise above $\Phi_I \approx 2 \times 10^{14}$ ions/cm^2 is in stark contrast to the trend that was observed for CO, where Y, after peaking at $\Phi_I \approx 5 \times 10^{14}$ ions/cm^2, steadily decreases. It was argued that this decrease is the result of a buildup of nonvolatile carbon-rich species with very high T_c. It seems clear that such buildup is resisted in CO_2 because of the abundance of O atoms. These can rapidly recombine with the carbon-rich species by highly exothermic reactions to reform CO and CO_2, thus stabilizing the composition of the target.

4.4.2. N_2O

$$N_2O \rightarrow N_2 + O(^1D) \qquad \Delta H = 3.70 \text{ eV} \qquad (17)$$

$$N_2O \rightarrow N + NO \qquad \Delta H = 5.00 \text{ eV} \qquad (18)$$

$$N_2O \rightarrow 2N + O(^1D) \qquad \Delta H = 13.50 \text{ eV} \qquad (19)$$

$$N + N_2O \rightarrow N_2 + NO \qquad \Delta H = -4.80 \text{ eV} \tag{20}$$

$$O(^1D) + N_2O \rightarrow 2NO \qquad \Delta H = -3.50 \text{ eV} \tag{21}$$

$$O(^1D) + N_2O \rightarrow O_2 + N_2 \qquad \Delta H = -5.39 \text{ eV} \tag{22}$$

The sputtering products of N_2O have been investigated [12,24] by IR examination of both the ejected material that has been collected on a cold window and of the residual solid of bombarded matrices. The primary product in each method was found to be NO (or N_2O_2) as would be expected for the reactions listed. E_{chem} is estimated as 1795 eV [(197 N atoms × −4.80 eV) + (191/2 O atoms × −3.50 eV) + (191/2 O atoms × −5.39 eV). This is over three times the value for CO_2, and N_2O indeed has a Y_0 value of 516 molecules/ion, more than twice that of CO_2.

For $\Phi_I > 0$, Y shows a small initial increase that peaks quickly at about $\Phi_I = 1 \times 10^{14}$ ions/cm^2, then decreases until $\Phi_I = 2 \times 10^{14}$ ions/cm^2, and subsequently remains constant at $Y = 525$ molecules/ion. This is consistent with the build up of various N_xO_y molecules of lower volatility by reactions such as:

$$O(^1D) + NO \rightarrow NO_2 \qquad \Delta H = -5.14 \text{ eV} \tag{23}$$

$$O(^1D) + NO_2 \rightarrow NO_3 \qquad \Delta H = -4.17 \text{ eV} \tag{24}$$

$$NO + NO_2 \rightarrow N_2O_3 \qquad \Delta H = -0.40 \text{ eV} \tag{25}$$

$$NO_3 + NO_2 \rightarrow N_2O_5 \qquad \Delta H = -0.95 \text{ eV} \tag{26}$$

The occurrence of these reactions is supported by the secondary ion mass spectrum of solid N_2O [25,26], which is particularly rich in N_2O_3 and N_2O_4.

4.4.3. NO_2

This molecule exists as the weakly bound dimer N_2O_4 in the solid state, and in the following we assume that all collisions that lead to dissociation also split the dimer. We can then write the dissociation reactions as if we were dealing with NO_2 itself by including the energy required to split the dimer (0.59 eV) as part of each value of D. This assumption is in agreement with the "spectator" collision model adopted in deriving Eqs. (3)–(5) and means that dissociation products of NO_2 will not remain bonded to the (undamaged) spectator NO_2 partner in the dimer

$$2NO_2 \rightarrow N_2O_4 \qquad \Delta H = -0.59 \text{ eV} \tag{27}$$

$$NO_2 \rightarrow O(^1D) + NO \qquad \Delta H = 5.14 \text{ eV} \tag{28}$$

$$NO_2 \rightarrow 2O(^1D) + N \qquad \Delta H = 13.64 \text{ eV} \tag{29}$$

$$O(^1D) + N_2O_4 \rightarrow N_2O_5 \qquad \Delta H = -4.53 \text{ eV} \tag{30}$$

$$NO + N_2O_4 \rightarrow NO_2 + N_2O_3 \qquad \Delta H = 0.19 \text{ eV} \tag{31}$$

$$N + N_2O_4 \rightarrow NO + N_2O_3 \qquad \Delta H = -3.17 \text{ eV} \tag{32}$$

The sputtering products of NO_2 have also been investigated [12,24] by the methods used for N_2O. The primary product in this case was found to be the asymmetric isomer of N_2O_3, again consistent with the reactions listed. We calculate E_{chem} to be 1311 eV [(271 O atoms × −4.53 eV) + (194 NO molecules × 0.19 eV) + (38 N atoms × −3.17 eV)], between that for CO_2 and N_2O. It is satisfying that the observed $Y_0 = 442$ molecules/ion also is between that for CO_2 and N_2O. The sputtering yield rises only slightly with fluence, again most likely because of the buildup of various N_xO_y molecules.

4.4.4. CH_4 and C_2H_4

These two condensed gas targets differ quite strongly in their physical characteristics: C_2H_4 has a 1.5–2 times larger mass, U, T_c, and S, than CH_4 (cf. Table 1). Nevertheless, their Y_0 values are comparable. This behavior can be understood by considering

Y_{casc}, Eq. (2), where it is seen that the effects of higher U and S almost cancel. In fact, for these two materials the measured Y_0 are almost identical with their Y_{casc}. This indicates that here the gas-flow sputtering contribution is negligible. The reason lies in the fact that the collision cascades in these rather low-density materials tend to be quite extended, and the energy density is not high enough to reach T_c and thereby initiate gas flow. Further, it appears that there is no help from E_{chem}. The expected reactions for CH_4 are

$$CH_4 \rightarrow CH_3 + H \qquad \Delta H = 4.55 \text{ eV} \qquad (33)$$

$$CH_4 \rightarrow C + 2H_2 \qquad \Delta H = 8.20 \text{ eV} \qquad (34)$$

$$H + CH_4 \rightarrow CH_3 + H_2 \qquad \Delta H = 0.03 \text{ eV} \qquad (35)$$

$$C + CH_4 \rightarrow C_2H_4 \qquad \Delta H = -6.11 \text{ eV} \qquad (36)$$

The neutral material sputtered from solid CH_4 by 6 keV Ar^+ ions has been reported [27e] to be primarily H_2 and CH_4 and smaller amounts of the C_2 species, C_2H_6, C_2H_4 (dominant), and C_2H_2, again consistent with the reactions listed. We find $E_{chem} = 79$ eV [(412 H atoms $\times$ 0.03 eV) + (15 C atoms $\times$ −6.11 eV)]. Similar reactions occur for C_2H_4 except that now the reaction of H atoms with the surrounding target molecules

$$H + C_2H_4 \rightarrow C_2H_5 \qquad \Delta H = -1.57 \text{ eV} \qquad (37)$$

is considerably exothermic [cf. reaction (35)], and $E_{chem} = 938$ eV.

The fluence dependence of Y for CH_4 under bombardment with 1–5 keV Ne^+ ions is displayed in Fig. 2(a). For all projectiles we observe a considerable initial increase in Y. This can be attributed to the gradual accumulation of highly volatile and easily sputtered H_2 by reactions (33)–(35), the combination of two H atoms after gas flow has ceased.

For higher fluences two different scenarios are seen to develop in Fig. 2. (1) Under light ion bombardment [shown in Fig. 2(a) for Ne^+ ions, but observed also for He^+ ions], the yields reach a maximum and then start decreasing. Such behavior has been observed repeatedly under higher keV- and MeV-ion bombardment of CH_4 and has been attributed to the formation of high-molecular-weight carbonaceous molecules in the target [27]. For the reactions considered up to now, it has been sufficient to start with only the neutral primary products. This is not likely to be the case here. If we begin with neutral reaction (33), a CH_3 radical can abstract a hydrogen atom from CH_4 in an energetically neutral reaction, but cannot condense with it to form a C_2H_x species. Two CH_3 radicals could combine to form C_2H_6, but this is infrequent and ignored presently. If we begin with reaction (34), we have similar problems. Atomic carbon can attack CH_4 to give C_2H_4 [reaction (36)]. This in turn can be attacked by CH_3 or C to give C_3H_x species, but the reactions can continue only if further CH_3 or C are encountered. The same problem arises if we were to start with CH_2 (if only two hydrogens are ejected from CH_4); the reaction stops with C_2H_6. In contrast, the reaction of CH_4 with the charged species CH_3^+ and H^+ is well suited to producing polymers by the sequence:

$$H^+ + CH_4 \rightarrow CH_5^+ \qquad \Delta H = -5.63 \text{ eV} \qquad (38)$$

$$CH_5^+ \rightarrow CH_3^+ + H_2 \qquad \Delta H = 1.90 \text{ eV} \qquad (39)$$

$$CH_3^+ + CH_4 \rightarrow C_2H_7^+ \qquad \Delta H = -0.71 \text{ eV} \qquad (40)$$

$$C_2H_7^+ \rightarrow C_2H_5^+ + H_2 \qquad \Delta H = -0.51 \text{ eV} \qquad (41)$$

$$C_2H_5^+ + CH_4 \rightarrow C_3H_9^+ \qquad \Delta H = -0.17 \text{ eV} \qquad (42)$$

etc.

(2) For heavier projectiles [shown in Fig. 1(b) for Ar^+ ions, but observed also for Kr^+ and Xe^+ ions] we see a saturation of the Y value at a high level, with no sign of a subsequent decrease. This behavior has not been observed before. We attribute it to a strong gas flow occurring under these higher yield conditions. Evidently, the flow is sufficient to entrain enough products to prevent the accumulation of larger polymers.

Note that projectiles of equal energy but different mass create distinctly different energy densities in the impact region. For example, for 5 keV Ne^+ and Ar^+ ion impact, using the appropriate values in Eqs. (7) and (8) for the cross-section constant C_m, $m = 0.25$, we obtain

$\rho = 123$ Å, $T = 83$ K

for 5 keV Ar^+ ion bombardment (43)

$\rho = 164$ Å, $T = 43$ K

for 5 keV Ne^+ for bombardment (44)

Here, cross sections for CH_4 and a low-temperature specific heat of $3k_B$/molecule, i.e. no vibrational excitation, have been assumed. The essential point is that the energy densities (temperatures) reached under Ne^+ ion bombardment can be a factor of two smaller than when Ar^+ ions are used.

Both temperatures are below the T_c of CH_4 (191 K), and a gas-flow contribution to sputtering in the virgin CH_4 target is not expected. However, the developing H_2 will effectively decrease bonding in the target and diminish the temperature necessary for flow development. Further, after prolonged bombardment, the enhanced stopping power of the larger C_xH_y molecules will increase T to the same effect. This will only occur, of course, if the ion-modified material has an atom-number density that is comparable to the original volume.

Even the light He^+ projectile leads to considerable fluence evolution of the sputtering yield and must be assumed to induce target material modifications. This is probably due to the good energy coupling of the He^+ ion to the H atoms that are abundant.

Fig. 2(b) shows that qualitatively analogous processes occur in a C_2H_4 target. The initial increase is again attributed to H_2 buildup. Now, due to the higher T_c of C_2H_4, even Ar^+ ions are unable to produce a sufficiently high energy density to establish the strong gas flow necessary to sputter the high-mass polymer products. However, bombardment with Kr^+ and Xe^+ ions [Fig. 2(c)] shows that the same high plateau yields as seen for CH_4 targets can be obtained.

4.4.5. NH_3

The bombardment of NH_3 can be usefully compared to that of CH_4 since both molecules have similar masses and stopping cross sections. The observed Y_0 values for NH_3 are similar to, but slightly higher than, those for CH_4, (Table 1). This appears to be due to a cancellation of two effects. The higher U and T_c of NH_3 make it less volatile and suppress both collision-cascade and gas-flow contributions to sputtering, but the density of NH_3 is 50% higher than that of CH_4. This causes the linear dimensions of the cascade to shrink by a factor of 67% [Eq. (1)], the energy density increases by a factor of $1.5^3 = 3.4$, and the sputtering of NH_3 has a high yield. As the comparison with the Y_{casc} in Table 2 shows, sputtering in NH_3 must be due, in large part, to a gas flow contribution. As for CH_4, the sputtering of NH_3 is expected to gain little or nothing from E_{chem}. The anticipated reactions are

$$NH_3 \rightarrow NH_2 + H \qquad \Delta H = 4.71 \text{ eV} \qquad (45)$$

$$NH_3 \rightarrow N + H_2 + H \qquad \Delta H = 7.63 \text{ eV} \qquad (46)$$

$$N + NH_3 \rightarrow N_2H_3 \qquad \Delta H = -0.65 \text{ eV} \qquad (47)$$

$$H + NH_3 \rightarrow H_2 + NH_2 \qquad \Delta H = 0.19 \text{ eV} \qquad (48)$$

Support for the validity of these reactions is provided by the neutral material which has been observed [28] to be sputtered from solid NH_3 by 3 keV Ar^+ ions—primarily NH_3, H_2, and N_2, and some N_2H_4. From these reactions, $E_{chem} = -62$ eV, i.e. actually slightly endothermic [(375 H atoms × 0.19 eV) + (14 N atoms × −0.65 eV)]. As displayed in Fig. 1(b), sputtering for NH_3 increases rapidly with increasing Φ_I. In analogy to CH_4 bombardment, this may again be attributed to the buildup of H_2. In contrast to CH_4 (and C_2H_4), however, NH_3 does not polymerize (i.e. reactions comparable to reactions (40)–(42) do not occur) and the yields do not subsequently decline. Instead, they saturate at relatively large values for reasons discussed above for CH_4.

5. Conclusions

We have measured the fluence dependence of the sputtering yields of the molecular-gas targets CO_2, NO_2, N_2O, NH_3, CH_4, and C_2H_4 under bombardment by rare gas ion in the keV energy range. The results are interpreted using concepts from collision cascade theory, the gas-flow model of sputtering, and the energetics of the expected chemical reactions.

For the three triatomic molecules studied, the physical properties (mass, atomic charges, density, and to a lesser extent, volatility) are similar, and the difference in the initial yields observed could be correlated to the exothermic chemical reactions that feed energy into the gas flow. The sputtering yield of CO_2 was found to be low, close to the calculated collision cascade yield, consistent with the fact that CO_2 is the lowest energy molecule that can be formed from carbon and oxygen. The sputtering yields of NO_2 and N_2O increase above that of CO_2 in proportion to the exothermicity of the chemical reactions occurring during and after ion impact. Only moderate fluence dependencies were observed, indicating that only modest chemical modifications build up on the surface of the target.

Bombardment of CH_4 and C_2H_4 targets resulted in low initial sputtering yields, implying that little or no gas flow participates in the sputtering mechanism. With prolonged bombardment, the sputtering yields rise in all cases studied due to the build-up of the highly volatile H_2. For higher bombardment fluences, however, two different trends are observed. In the case of lighter ions (He^+, Ne^+, and for C_2H_4 targets, also Ar^+) the yields eventually decrease, probably due to polymerization reaction products coating the surface of the target. For heavier projectile ions, however, the yields saturate at a high level. We attribute this latter behavior to a large gas-flow contribution to the sputtering mechanism which erodes even the heavier carbonaceous products.

The results for NH_3 are similar to those for CH_4 and C_2H_4, except that there is no buildup of polymers on the surface of the target. Thus, the yields do not decrease with increasing incident ion fluence.

Acknowledgements

This work was supported by the NSF (CHE 9819179).

References

[1] R.E. Johnson, Energetic Charged-Particle Interactions with Atmospheres and Surfaces, Springer, Berlin, 1990.
[2] J. Schou, Nucl. Instrum. Methods Phys. Res. B 27 (1987) 188.
[3] D.J. Oostra, A.E. de Vries, Nucl. Instrum. Methods Phys. Res. B 18 (1987) 618.
[4] C.F. Abrams, D.B. Graves, J. Appl. Phys. 86 (1999) 5938.
[5] H.M. Urbassek, K.T. Waldeer, Phys. Rev. Lett. 67 (1991) 105.
[6] H.H. Andersen, Mat. Fys. Medd. Dan. Vid. Selsk. 43 (1993) 127.
[7] R.E. Johnson, J. Schou, Mat. Fys. Medd. Dan. Vid. Selsk. 43 (1993) 403.
[8] V. Balaji, D.E. David, T.F. Magnera, J. Michl, H.M. Urbassek, Nucl. Instrum. Methods Phys. Res. B 13 (1990) 435.
[9] V. Balaji, D.E. David, R. Tian, J. Michl, H.M. Urbassek, J. Phys. Chem. 99 (1995) 15565.
[10] H.E. Roosendaal, R.A. Haring, J.B. Sanders, Nucl. Instrum. Methods 194 (1982) 579.
[11] P. Sigmund, C. Claussen, J. Appl. Phys. 52 (1981) 990.
[12] D.E. David, T.F. Magnera, R. Tian, J. Michl, Radiat. Eff. 99 (1986) 731.
[13] D.E. David, T.F. Magnera, R. Tian, D. Stulik, J. Michl, Nucl. Instrum. Methods Phys. Res. B 14 (1986) 378.
[14] J. Michl, Int. J. Mass Spectrom. Ion Phys. 53 (1983) 255.
[15] H.M. Urbassek, J. Michl, Nucl. Instrum. Methods Phys. Res. B 22 (1987) 480.
[16] P. Sigmund, Sputtering by Particle Bombardment 1, R. Behrisch (Ed.), Springer, Berlin, 1981, p. 9.
[17] P.C. Zalm, J. Appl. Phys. 54 (1983) 2660.
[18] R.L. Hudson, M.H. Moore, J. Phys. Chem. 96 (1992) 6500.
[19] W.G. Mallard, F. Westley, J.T. Herron, R.F. Hampson, D.H. Frizzell, NIST Chemical Kinetics Database, Windows Version 2Q98, National Institute of Standards and Technology, Gaithersburg, MD, 1998.
[20] NIST Chemistry WebBook, NIST Standard Reference Database Number 69, W.G. Mallard, P.J. Linstrom (Eds.), National Institute of Standards and Technology, Gaithersburg, MD, 2000 (http://webbook.nist.gov).
[21] R. Pedrys, D.J. Oostra, A.E. de Vries, Desorption Induced by Electronic Transitions, DIETS II, W. Brenig, D. Menzel (Eds.), Springer Series in Surface Science Vol. 4, Springer, Berlin, 1985, p. 190.
[22] M. Kertesz, R. Hoffman, J. Am. Chem. Soc. 106 (1984) 3453.
[23] R.G. Orth, H.T. Jonkman, J. Michl, Int. J. Mass Spectrom. Ion Phys. 43 (1982) 441.
[24] R. Tian, Ph.D. dissertation, Reaction mechanisms for bombarded frozen gases. University of Utah (1988).
[25] R.G. Orth, H.T. Jonkman, J. Michl, J. Am. Chem. Soc. 104 (1982) 1834.
[26] R.G. Orth, H.T. Jonkman, J. Michl, J. Am. Chem. Soc. 103 (1981) 1564.
[27] (a) J. Benit, J.P. Bibbing, F. Rocard, Nucl. Instrum. Methods Phys. Res. B 32 (1988) 349; (b) G. Foti, L. Calcagno, F.Z. Zhou, G. Strazzulla, ibid. 24/25 (1987) 522; (c) R. Pedrys, D.J. Oostra, R.A. Haring, L. Calcagno, A. Haring, A.E. de Vries, ibid. 17 (1986) 15; (d) L. Calcagno, G. Foti, L. Torrisi, G. Strazzulla, Icarus 63 (1985) 31; (e) G. Strazzulla, L. Calcagno, G. Foti, Nuovo Cimento Soc. Ital. Fis. 8C (1985)

63; (f) W.L. Brown, L.J. Lanzerotti, J.E. Bower, G. Foti, R.E. Johnson, Nucl. Instrum. Methods Phys. Res. B 19/20 (1987) 899.

[28] R.A. Haring, R. Pedrys, D.J. Oostra, A. Haring, A.E. de Vries, Nucl. Instrum. Methods Phys. Res. B 233, (1984) 476; A.E. de Vries, R.A. Haring, A. Haring, F.S. Klein, A.C. Kummel, F.W. Saris, J. Phys. Chem. 88 (1984) 4510; R.A. Haring, A. Haring, F.S. Klein, A.C. Kummel, A.E. de Vries, Nucl. Instrum. Methods 211 (1983) 529.

[29] CRC Handbook of Thermophysical and Thermochemical Data, D.R. Lide, H.V. Kehiaian, (Eds.), CRC Press, Boca Raton, FL, 1994.

[30] C.L. Yawls, Thermodynamics and Physical Property Data, Gulf Publishing, Houston, 1992.

[31] G.W.C. Kaye, T.H. Laby, Tables of Physical and Chemical Constants, Longman, 1995.

[32] P.E. Liley, T. Mahita, Y. Tauch, Properties of Inorganic and Organic Fluids, Hemisphere, New York, 1988.